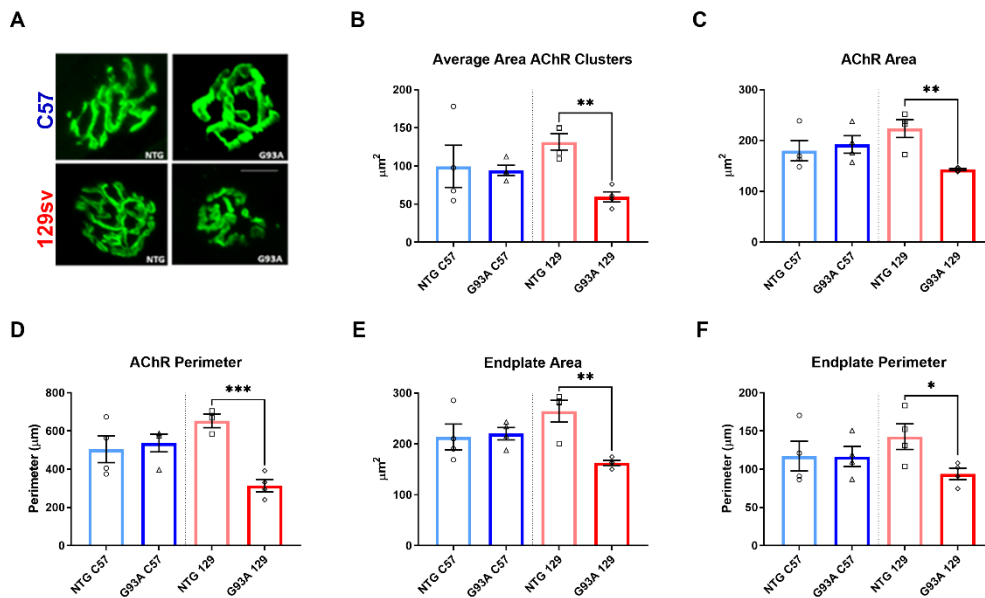
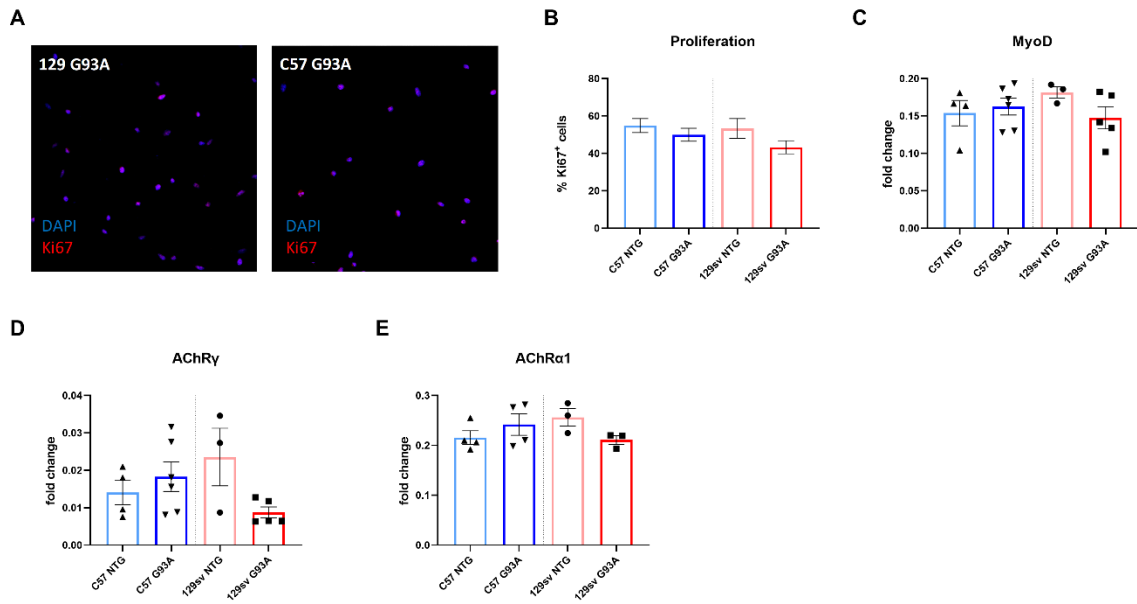


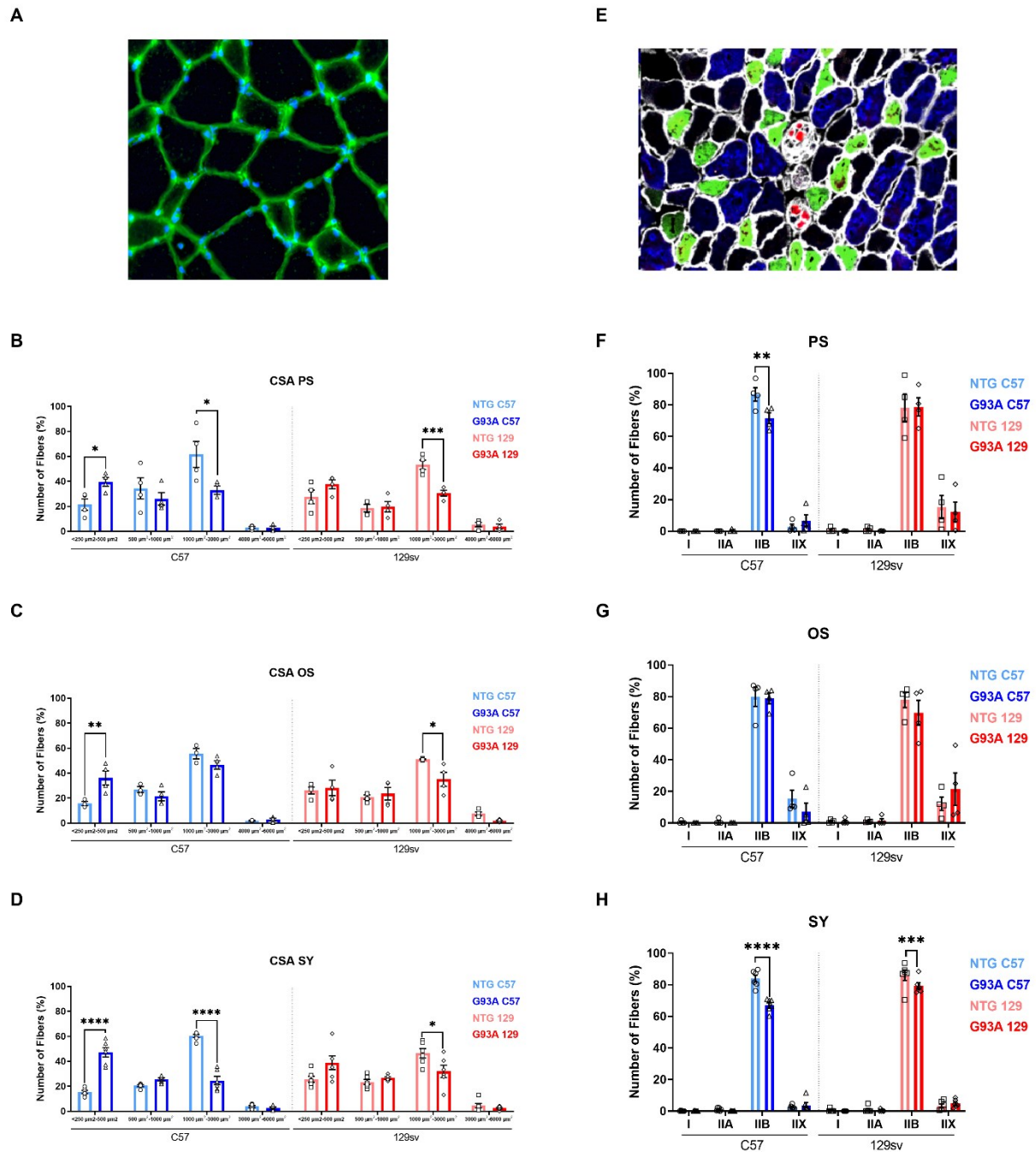
Supplementary Fig. 1. Skeletal muscle SOD1 expression and late muscle denervation in fast and slow progressing SOD1^{G93A} mice. (A and B) Representative Immunoblot image and relative densitometric analysis of soluble and aggregated human and murine SOD1 protein expression in GCM muscles of C57SOD1^{G93A} and 129SvSOD1^{G93A} mice compared with NTG littermates ($n = 4$). Protein levels were normalised on the total amount of protein loaded. Data are expressed as the mean (\pm SEM) and analysed by 2-way ANOVA with uncorrected Fisher's LSD post-analysis.



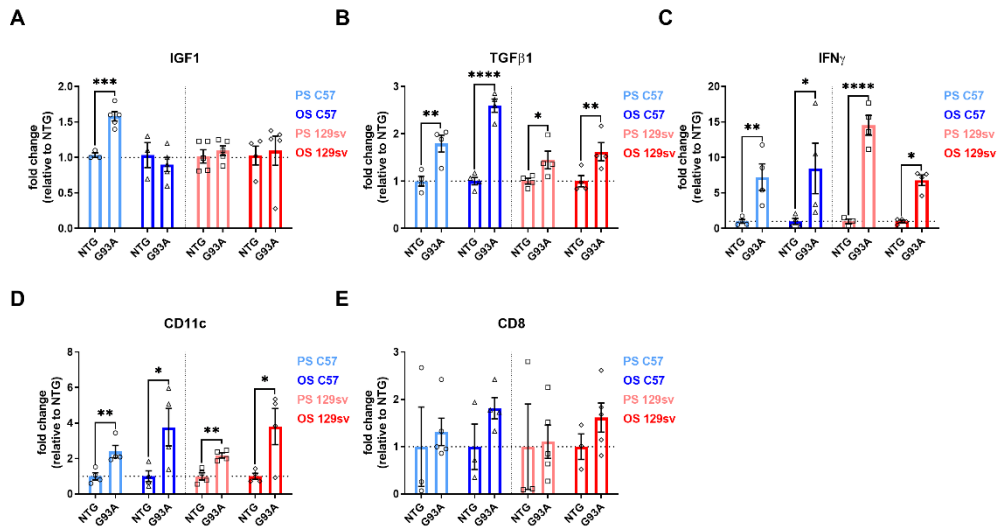
Supplementary Fig. 2. Nicotinic Acetylcholine receptor morphology in fast and slow progressing mice. (A) Representative confocal micrographs and morphometric analysis of α -Bungarotoxin (BTX) positive endplates on longitudinal sections of GCM in C57SOD1^{G93A} mice, 129SvSOD1^{G93A} mice and NTG littermates at 12 weeks of age. **(B-F)** Average area clusters **(B)**, AChR area **(C)**, AChR perimeter **(D)**, Endplate area **(E)** and Endplate perimeter **(F)** have been analysed through NMJ-Morph ($n = 4$). Data are expressed as the mean (\pm SEM). Significance was calculated with Two-way ANOVA with uncorrected Fisher's LSD post-analysis ($*P \leq 0.05$; $**P \leq 0.01$; $***P \leq 0.001$).



Supplementary Fig. 3. Ex-vivo muscle-derived satellite cells proliferation in fast and slow-progressing mice. (A) Representative confocal micrographs showing the immunostaining for Ki67 (red) and DAPI (blue) on primary satellite cell (SC) cultures of C57SOD1^{G93A} and 129SvSOD1^{G93A} mice in growing medium for 72 h, compared with NTG littermates. Scale bar = 100 μm. (B) The proliferation index was calculated as No. of Ki67 and DAPI positive cells ($n = 3$). Data are reported by means \pm SEM. Statistics were calculated by One-way ANOVA with uncorrected Fisher's LSD post-analysis. (C-E) Real-time qPCR for MyoD (C), AchR γ (D) and AchR α 1 (E) mRNA transcripts in primary SC cultures of C57SOD1^{G93A} and 129SvSOD1^{G93A} mice compared with NTG littermates ($n = 3$). Data are expressed as the mean (\pm SEM). Data were analysed by Two-way ANOVA with uncorrected Fisher's LSD post-analysis.



Supplementary Fig. 4. Muscle fibre composition of the two ALS murine models. (A and D) Representative confocal micrograph and longitudinal analysis of Lectin immunostained muscle fibre cross-sectional area (CSA) on GCM coronal sections of C57SOD1^{G93A} mice 129svSOD1^{G93A} mice and relative NTG littermates ($n = 6$). For each section, the percent of fibre dimension was calculated relative to the total number of muscle fibres counted by Muscle J. Data are expressed as the mean (\pm SEM). Significance was calculated with 2-way ANOVA with uncorrected Fisher's LSD post-analysis ($*P \leq 0.05$; $***P \leq 0.001$; $****P \leq 0.0001$). (E and H) Representative confocal micrograph and longitudinal analysis of fibre type composition on GCM coronal sections of C57SOD1^{G93A} mice 129svSOD1^{G93A} mice and NTG littermates ($n = 6$). A mix of antibodies against I (red), IIA (green), IIB (blue), MyHCs and Lectin (white) were used; IIX muscle fibres are unstained (black). Percent of fibre types was calculated relative to the total number of muscle fibres counted by Muscle J. Data are expressed as the mean (\pm SEM). Significance was calculated with Two-way ANOVA with uncorrected Fisher's LSD post-analysis ($**P \leq 0.01$).



Supplementary Fig. 5. Muscle inflammatory signals in fast and slow progressing mice. (A-D) Real-time qPCR for IGF1 (A), TGFβ1 (B), IFNγ (C), CD11c (D) and CD8 (E) mRNA transcripts in GCM muscle of C57SOD1^{G93A} and 129SvSOD1^{G93A} mice compared with NTG littermates ($n = 4$). Data are expressed as the mean (\pm SEM). Significance was calculated with Two-way ANOVA with uncorrected Fisher's LSD post-analysis ($*P \leq 0.05$; $**P \leq 0.01$; $***P \leq 0.001$; $****P \leq 0.0001$).